Analysis of spontaneous oscillations for a three-state power-stroke model

Takumi Washio* and Toshiaki Hisada
Graduate School of Frontier Sciences, The University of Tokyo, 178-4 Wakashiba, Kashiwa, Chiba 277-0871, Japan

Seine A. Shintani and Hideo Higuchi
Department of Physics, Graduate School of Science, The University of Tokyo, 7-3-1 Hongo, Bunkyo-ku, Tokyo 113-0033, Japan
(Received 18 July 2016; revised manuscript received 31 October 2016; published 21 February 2017)

Our study considers the mechanism of the spontaneous oscillations of molecular motors that are driven by the power stroke principle by applying linear stability analysis around the stationary solution. By representing the coupling equation of microscopic molecular motor dynamics and mesoscopic sarcomeric dynamics by a rank-1 updated matrix system, we derived the analytical representations of the eigenmodes of the Jacobian matrix that cause the oscillation. Based on these analytical representations, we successfully derived the essential conditions for the oscillation in terms of the rate constants of the power stroke and the reversal stroke transitions of the molecular motor. Unlike the two-state model, in which the dependence of the detachment rates on the motor coordinates or the applied forces on the motors plays a key role for the oscillation, our three-state power stroke model demonstrates that the dependence of the rate constants of the power and reversal strokes on the strains in the elastic elements in the motor molecules plays a key role, where these rate constants are rationally determined from the free energy available for the power stroke, the stiffness of the elastic element in the molecular motor, and the working stroke size. By applying the experimentally confirmed values to the free energy, the stiffness, and the working stroke size, our numerical model reproduces well the experimentally observed oscillatory behavior. Furthermore, our analysis shows that two eigenmodes with real positive eigenvalues characterize the oscillatory behavior, where the eigenmode with the larger eigenvalue indicates the transient of the system of the quick sarcomeric lengthening induced by the collective reversal strokes, and the smaller eigenvalue correlates with the speed of sarcomeric shortening, which is much slower than lengthening. Applying the perturbation analyses with primal physical parameters, we find that these two real eigenvalues occur on two branches derived from a merge point of a pair of complex-conjugate eigenvalues generated by Hopf bifurcation.

DOI: 10.1103/PhysRevE.95.022411

I. INTRODUCTION

The movement of skeletal and cardiac muscles is fundamentally regulated by the transients of intracellular calcium concentration, which is triggered by the electrical stimulation of cells. A spontaneous oscillation is the oscillatory behavior of a single myofibril (sarcomere) generated without such transients of calcium concentration. Spontaneous oscillation is an interesting research topic not only for insect flight muscles of asynchronous type [1] but also cardiac muscles because such a phenomenon has been experimentally observed in specific conditions [2,3]. These facts suggest that the mechanism of muscle relaxation in a spontaneous oscillation may also serve for the quick relaxation in regulated heartbeats because the fall of blood pressure is fast for a healthy heartbeat despite the slow decline of intracellular calcium concentration [4]. Such quick relaxation is important to enable the quick blood filling to the ventricles during the diastolic phase. Thus, seeking the sources of oscillation is an important issue, even for the muscles whose state transition from contraction to relaxation is regulated by calcium signals. In typical numerical modeling, sarcomere movement is represented by the change of sarcomere length from its unloaded state, where a certain elasticity is assumed for this length displacement [5]. The contraction force acting on the sarcomere is given by the sum of forces generated by the myosin molecules that pull the actin filaments connected to the Z-disk located at the sarcomere edge. Thus, one-dimensional models [4–9] have been adopted to analyze sarcomere movement, where the sarcomere length displacement is the mesoscopic variable. Microscopic variables consist of a number of functions $\{p_S(x)\}$, where each function p_S represents the probability density with respect to a domain variable x in the specific state S of the molecular motors. In such a situation, a number of models that produce oscillations have been proposed [10–13]. For example, Jülicher *et al.* [10] showed that a simple two-state (consisting of the nonbinding and binding states) molecular motor model is capable of reproducing an oscillation, and they developed the criteria of oscillation based on linear stability analysis at its stationary solution. In their model, the domain variable x is the periodically iterated coordinate along a polar filament used to represent a periodic potential function that generates the pulling force for the attached molecular motors. Furthermore, the two-state model has been successfully applied to explain more complicated phenomena, such as spontaneous waves in muscle fibers [11], subharmonic oscillations in an *in vitro* actomyosin system [12], and the chaotic behavior of sarcomere [13]. However, because the contraction forces should be generated by the power strokes of the binding myosin molecules [14–17], it is necessary to study the mechanism of spontaneous oscillations in relation to the power stroke principle if this principle is closely related to the oscillation mechanism.

*Author to whom all correspondence should be addressed: washio@sml.k.u-tokyo.ac.jp

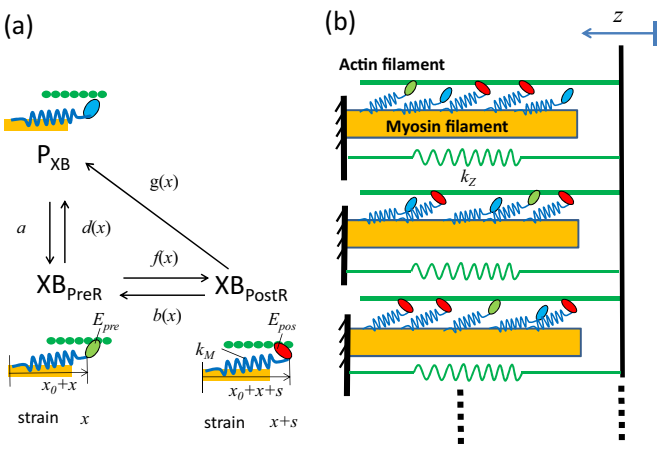

FIG. 1. (a) The numerical three-state power stroke model and (b) the half sarcomere model. At the transitions between the binding states (XB_{preR}, XB_{postR}), the strain of the elastic element is changed by stroke size s (nm), and the rate constants of these transitions depend on the strain. x_0 is the natural length of the elastic element.

In our model [Fig. 1(a)], we assume that the pulling forces are given by the strain (x) of the elastic arms in the myosin molecules binding to the actin filament, and this strain increases by the working stroke size s in the forward transition from the prestroke state to the poststroke state (power stroke), whereas it decreases by s in the backward transition from the poststroke state to the prestroke state (reversal stroke). The rate constant of the forward (f) and backward (b) transitions between the pre- and poststroke states, with strains x and $x+s$, respectively, is determined as it follows from the relationship given by the statistical equilibrium:

$$\frac{f(x)}{b(x)} = \exp\left(\frac{-\Delta E(x)}{kT}\right), \tag{1}$$

where $\Delta E(x)$ is the difference between the total energy at the poststroke state and that at the prestroke state:

$$\Delta E(x) = E_{\rm pos} + \tfrac{1}{2}k_M(x+s)^2 - E_{\rm pre} - \tfrac{1}{2}k_M x^2, \tag{2}$$

where we assume linear elasticity with the spring constant k_M (=2.8 pN/nm) [14] for the strain in the elastic myosin arm. $E_{\rm pre}$ and $E_{\rm pos}$ are free energies in the myosin head at the pre- and poststroke states, respectively. k and T denote the Boltzmann constant and absolute temperature, respectively. We simulate the contraction in body temperature; therefore, we assume $kT = 4.28$ pN nm. This molecular model is coupled with the sarcomeric movement described by the shortening displacement variable z [Fig. 1(b)] from the unloaded sarcomere length. For the individual binding myosin, its strain x is changed by $-dz/dt$ per unit time; therefore, sarcomere shortening results in the shift of density given by

$$\delta p_S(t,x) = \frac{dz}{dt}\frac{\partial p_S}{\partial x}(t,x)\delta t. \tag{3}$$

In this way, the change of mesoscopic variable z shifts the density in the molecular state, thereby affecting the state transitions between the pre- and poststroke states. Additionally, the changes of the state transitions vary the pulling forces of the binding myosin molecules in turn. We show that this coupling of mesoscopic sarcomeric movement and microscopic molecular state transitions can be regarded as the rank-1 update of the matrix system that represents only the state transition under the isometric condition. Based on this matrix representation, we derive an analytical representation of the eigenmodes that cause instability at the stationary solution. This analytical representation of the unstable eigenmode includes the rate constants of the transitions between the three states in a relatively simple manner. Therefore, we can discuss the causes of the oscillation from various views, not only of the power stroke parameters but also the attachment and detachment parameters.

In the two-state model, the causes of oscillations are closely related to the detachment rates that depend either on the motor coordinate along the filament [10,12] or the force applied to the motor molecule [13]. For these two cases of the two-state model, an adenosine triphosphate (ATP) molecule is consumed at any detachment. In particular, for the latter case, the increase of the detachment rate with the increase of the applied force is not energetically preferable because the strain energy preserved in the elastic element is discarded after it consumes one ATP molecule. By contrast, there are two reaction pathways of detachment from the poststroke state in the three-state model. One is the direct transition to the nonbinding state in which one ATP molecule is consumed, and the other is the detachment via the prestroke state mediated by the reversal stoke, where the ATP molecule is not consumed. We show that quick relaxation in spontaneous oscillations is induced by the collective detachments given by the latter pathway, where no ATP molecules are consumed. Although the second pathway may be interpreted as the load dependent detachment in the two-stroke model, discriminating between the two pathways is essential when one wants to evaluate energy consumption. For example, one of our objectives in this work is to refine our molecular model when it is applied in beating heart simulations [4] through the benchmarking of the spontaneous oscillation found by Shintani *et al.* [3] for neonatal cardiomyocytes. For the case of applying such a heart simulator in medical applications, one of the great concerns of doctors is energy consumption. Thus, discriminating between the two detachments is necessary.

II. SARCOMERE MODEL

We consider the half-sarcomere model composed of the half thick (myosin) filaments and thin (actin) filaments, as shown in Fig. 1(b). The myosin filaments are fixed at one end to a wall, and the actin filaments are connected to the Z-disk at the opposite end. We assume that the wall and Z-disk are connected by the elastic components, with a spring constant k_Z per one actin filament that represents the sarcomeric stiffness. The position of the Z-disk is indicated by z, where the positive direction of z corresponds to the shortening of the sarcomere. As shown in Fig. 1(a), we assume that the myosin molecule has three conformations composed of one nonbinding state (P_{XB}) and two binding states (the prestroke state XB_{preR} and the poststroke state XB_{postR}). Each binding myosin head pulls the actin filament with force $k_M x$ determined by strain x in its elastic arm. In the transition from XB_{preR} to XB_{postR} (the forward transition), the strain is assumed to be elongated by

working stroke size s by the power stroke, whereas in the transition from XB_{postR} to XB_{preR} (the backward transition), the strain is assumed to be shortened by working stroke size s by the reversal stroke. In our mathematical analysis, we assume that the rate constants of these forward and backward transitions are given by functions f and b of strain x at XB_{preR}, respectively. Although we assume that the detachment rate constants d and g are also given as functions of strain x in the mathematical analysis, we adopt constants for them in our numerical tests in this paper. The attachment rate constant a is assumed to be a constant. However, the initial strain at the attachment follows the Boltzmann distribution as shown later in this section. We assume that there is a sufficiently large number of filaments so that the densities in the binding states can be approximated by the smooth functions p_{pre} and p_{pos} for XB_{preR} and XB_{postR}, respectively.

Under these assumptions, the transition at the nonbinding state P_{XB} is given as follows:

$$\frac{dP_{pxb}}{dt} = \int_{-\infty}^{+\infty} d(x)p_{pre}(t,x)dx + \int_{-\infty}^{+\infty} g(x)p_{pos}(t,x+s)dx - aP_{pxb}, \quad (4)$$

where P_{pxb} denotes the concentration of myosin molecules in P_{XB}. Hereafter, the integral region will always be $[-\infty, +\infty]$. Therefore, we will omit the integration range. The transitions of binding states XB_{preR} and XB_{postR} with strains x and $x+s$, respectively, are given as follows:

$$\frac{\partial p_{pre}}{\partial t}(t,x) = \frac{dz}{dt}(t)\frac{\partial p_{pre}}{\partial x}(t,x) + aP_{pxb}y_0(x) - d(x)p_{pre}(t,x) - f(x)p_{pre}(t,x) + b(x)p_{pos}(t,x+s) \quad (5)$$

$$\frac{\partial p_{pos}}{\partial t}(t,x) = \frac{dz}{dt}(t)\frac{\partial p_{pos}}{\partial x}(t,x+s) - g(x)p_{pos}(t,x+s) + f(x)p_{pre}(t,x) - b(x)p_{pos}(t,x+s). \quad (6)$$

We assume that the densities are normalized so that the sum of P_{pxb} and integrals of p_{pre} and p_{pos} are equal to 1. At the attachment, the initial arm strain is assumed to be given by density y_0, which is determined by the Boltzmann distribution defined by the strain energy of the myosin arm:

$$y_0(x) = \sqrt{\frac{k_M}{2\pi kT}}\exp\left(\frac{-k_M x^2}{2kT}\right). \quad (7)$$

The first terms on the right-hand sides of Eqs. (5) and (6) represent the shifts of densities caused by filament sliding, as shown in Eq. (3), where dz/dt is the shortening velocity of the half sarcomere. The rate constants f and b of the forward and backward transitions are assumed to be given as functions of strain x:

$$f(x) = r_{xb}\exp\left(\frac{E_{pre}+k_M x^2/2-E_c-k_M(x+s/2)^2/2}{kT}\right), \quad (8)$$

$$b(x) = r_{xb}\exp\left(\frac{E_{pos}+k_M(x+s)^2/2-E_c-k_M(x+s/2)^2/2}{kT}\right), \quad (9)$$

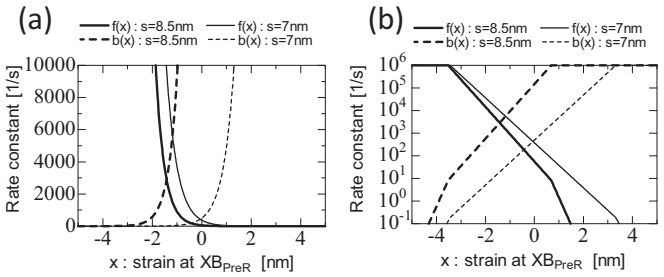

FIG. 2. The strain-dependent rate constants for the forward and backward transitions with (a) the normal scale and (b) log scale representations. The forward and backward rate constants $f(x)$ and $b(x)$ are plotted for the two cases with working stroke sizes $s =$ 8.5 nm (thick lines) and $s = 7$ nm (thin lines). These rate constants are shown with respect to strain x at the prestroke state. The other parameters are set as $r_{xb} = 10^5$ (1/s), $E_{pre} = 0.7E_{ATP}$, $E_c = 1.1E_{pre}$, and $E_{pos} = 0$.

where E_{pre} (=$0.7E_{ATP}$) and E_{pos} (=0) denote the free energies in the myosin head in the states XB_{preR} and XB_{postR}, respectively. We assume that 70% of the ATP hydrolysis energy (E_{ATP}) is consumed at the power stroke. E_c is the free energy at the potential barrier that separates the two states XB_{preR} and XB_{postR}. We assume that this barrier exists at the center of power-stroke distance s. We adopt $E_{ATP} = 22.5\,kT =$ 96.34 pN nm throughout this paper, which corresponds to 58 kJ/mol measured by Saupe *et al.* [18]. For the numerical stability of the explicit Euler scheme applied in our numerical simulations, if the maximum of $f(x)$ and $b(x)$ exceeds the limit r_{max} [=10^6 (1/s)] for given strain x, the maximum is reduced to r_{max} without changing the ratio $f(x) : b(x)$. Note that the rate constants in Eqs. (8) and (9) fulfill the thermal equilibrium condition given in Eq. (1). Although there are other approaches to define f and b that fulfill the equilibrium condition, we adopt the above definition because the Kramers-Smoluchovski approximation [19] suggests that the transition rate from state A to state B must be defined from the energy difference between the state of departure A and the barrier between A and B. In Fig. 2, these strain-dependent rate constants are shown for the two cases with different working stroke sizes ($s = 8.5$ and 7 nm) with respect to strain x at prestroke state XB_{preR}. For the case of $s = 8.5$ nm, the fluctuation zone, where both the forward and backward rate constants take values of the same order of magnitude, is located around $x = -1.5$ nm, whereas it is located around $x = 0$ nm in the case of $s = 7$ nm. The rate constants at the fluctuation zone for $s = 8.5$ nm are much larger than those for $s = 7$ nm. We selected the working stroke size $s = 7$ nm only for a comparison with $s = 8.5$ nm, which is close to the value $s = 8$ nm experimentally measured by Kaya and Higuchi [14].

To obtain the numerical results in this paper, the densities $p_{pre}(t,x)$ and $p_{pos}(t,x+s)$ were discretized on the finite strain space $[-3s,3s]$ of x with spatial spacing $\Delta x = s/100$. For the computation of the first derivatives $\partial p_{pre}/\partial x$ and $\partial p_{pos}/\partial x$, the third-order upwind scheme was adopted for stability, especially at the rapid stretching area. For the components of p_{pre} and p_{pos} outside $[-2s,2s]$, a large detachment rate equal to r_{max} was imposed because we assumed that these

myosins with extremely large strains detach immediately. For time marching, the explicit Euler scheme was used with time step size $\Delta t = 10^{-9}$ s.

As we show later in the paper, spontaneous oscillatory behavior similar to that observed by Shintani *et al.* [3] is reproduced well with $s = 8.5$ nm, whereas $s = 7$ nm seems to be too small to produce oscillations. In this paper, we analyze a coupled system of the above state transition model and sarcomeric movement governed by an equation of motion:

$$\gamma \frac{dz}{dt}(t) = n_M k_M \left(\int x p_{\mathrm{pre}}(t,x)dx + \int (x+s) p_{\mathrm{pos}}(t,x+s)dx \right) - k_Z z(t), \quad (10)$$

where γ is the viscosity coefficient per one actin filament in the half-sarcomere model imposed for filament sliding, n_M (=80) is the number of myosin molecules that can attach one actin filament, and k_Z denotes the spring constant per one actin filament. Note that k_Z represents passive sarcomeric stiffness, where the word "passive" means that this stiffness is measured in the relaxation state.

We combine the density functions at time t into one vector as follows:

$$\boldsymbol{p}(t) = \begin{bmatrix} \{\hat{p}_{\mathrm{pre}}\} \\ \{\hat{p}_{\mathrm{pos}}\} \\ P_{\mathrm{pxb}} \end{bmatrix}(t), \quad (11)$$

where the brackets {} denote the vector representing the density functions at time t, and the carets indicate these functions are defined for strain x at prestroke state $\mathrm{XB}_{\mathrm{preR}}$ as follows:

$$\hat{p}_{\mathrm{pre}}(x) \equiv p_{\mathrm{pre}}(t,x), \quad (12)$$

$$\hat{p}_{\mathrm{pos}}(x) \equiv p_{\mathrm{pos}}(t,x+s). \quad (13)$$

Note that the strain for poststroke density function $\hat{p}_{\mathrm{pos}}$ is given by $x + s$, where x is the strain at the prestroke state and s is the working stroke size. Under the above definitions, Eqs. (4)–(6), together with Eq. (10), are represented as

$$\frac{d\boldsymbol{p}}{dt}(t) = \frac{dz}{dt}(t)\boldsymbol{C}\,\boldsymbol{p}(t) - \boldsymbol{A}\,\boldsymbol{p}(t), \quad (14)$$

$$\frac{dz}{dt}(t) = \frac{1}{\gamma}[k_M \boldsymbol{B}\,\boldsymbol{p}(t) - k_Z z(t)], \quad (15)$$

where the operator $\boldsymbol{A}$ represents the state transitions given as

$$\boldsymbol{A} \equiv \begin{bmatrix} \langle f+d \rangle & \langle -b \rangle & -a\{y_0\} \\ \langle -f \rangle & \langle b+g \rangle & \{0\} \\ -\{d\}^T & -\{g\}^T & a \end{bmatrix}, \quad (16)$$

where the brackets denote the operators defined by

$$(\langle c \rangle \{\hat{p}\})(x) \equiv c(x)\hat{p}(x), \quad \forall\, x, \quad (17)$$

$$(\{c\}P)(x) \equiv Pc(x), \quad \forall\, x, \quad (18)$$

$$\{c\}^T\{\hat{p}\} \equiv \int c(x)\hat{p}(x)dx \quad (19)$$

for any function c of strain x at the prestroke state, any scalar P, and any density function $\hat{p}$. Note that the following equations hold for any functions c_1 and c_2, and these equations allow us to compute multiplications of these operators as usual scalar variables:

$$\langle c_1 \rangle \langle c_2 \rangle = \langle c_1 c_2 \rangle, \quad (20)$$

$$\langle c_1 \rangle \{c_2\} = \langle c_1 c_2 \rangle \{1\} = \{c_1 c_2\}, \quad (21)$$

$$\{c_1\}^T \langle c_2 \rangle = \{1\}^T \langle c_1 c_2 \rangle = \{c_1 c_2\}^T. \quad (22)$$

The operator $\boldsymbol{B}$ provides the integration of strains per one actin filament for a given density:

$$\boldsymbol{B}\,\boldsymbol{p} \equiv n_M \left(\int x\,\hat{p}_{\mathrm{pre}}(x)dx + \int (x+s)\hat{p}_{\mathrm{pos}}(x)dx \right), \quad \forall \boldsymbol{p} = \begin{bmatrix} \{\hat{p}_{\mathrm{pre}}\} \\ \{\hat{p}_{\mathrm{pos}}\} \\ P_{\mathrm{pxb}} \end{bmatrix}. \quad (23)$$

The operator $\boldsymbol{C}$ is the first-order spatial derivative acting on the two density functions defined by

$$\boldsymbol{C}\,\boldsymbol{p} \equiv \begin{bmatrix} \{\frac{d\hat{p}_{\mathrm{pre}}}{dx}\} \\ \{\frac{d\hat{p}_{\mathrm{pos}}}{dx}\} \\ 0 \end{bmatrix}, \quad \forall\, \boldsymbol{p} = \begin{bmatrix} \{\hat{p}_{\mathrm{pre}}\} \\ \{\hat{p}_{\mathrm{pos}}\} \\ P_{\mathrm{pxb}} \end{bmatrix}. \quad (24)$$

By applying Eq. (20), it can be shown that the kernel of the operator $\boldsymbol{A}$ is one-dimensional space spanned by the basis vector:

$$\boldsymbol{p}_0 \equiv \begin{bmatrix} \{\hat{p}_{\mathrm{pre},0}\} \\ \{\hat{p}_{\mathrm{pos},0}\} \\ P_{\mathrm{pxb},0} \end{bmatrix} \quad (25)$$

with

$$P_{\mathrm{pxb},0} = \frac{1}{a\int \frac{v(x)+f(x)}{e(x)} y_0(x)dx + 1}, \quad (26)$$

$$\hat{p}_{\mathrm{pre},0}(x) = p_{\mathrm{pre},0}(x) = P_{\mathrm{pxb},0}\frac{a v(x)}{e(x)} y_0(x), \quad (27)$$

$$\hat{p}_{\mathrm{pos},0}(x) = p_{\mathrm{pos},0}(x+s) = P_{\mathrm{pxb},0}\frac{a f(x)}{e(x)} y_0(x), \quad (28)$$

where the functions u, v, and e are defined by

$$u(x) \equiv f(x) + d(x), \quad (29)$$

$$v(x) \equiv b(x) + g(x), \quad (30)$$

$$e(x) \equiv u(x)v(x) - f(x)b(x). \quad (31)$$

The proof is provided in Appendix A.

This kernel vector corresponds to the stationary densities in the isometric contraction condition that correspond to $dz/dt = 0$, as shown later in this section. In Fig. 3, these stationary densities are shown with the coefficients multiplied to initial density y_0 in Eqs. (27) and (28) for the two working stroke sizes $s = 8.5$ and 7 nm. In the case of $s = 8.5$ nm [Fig. 3(a)], the majority of initial density y_0 represented as the alternate long and short dashed lines in the top panel is deleted by coefficient function $c_{\mathrm{pos}}(x) = P_{\mathrm{pxb},0} a f(x)/e(x)$ represented by the dashed line, except for the left edge around $x = -2$ nm in forming

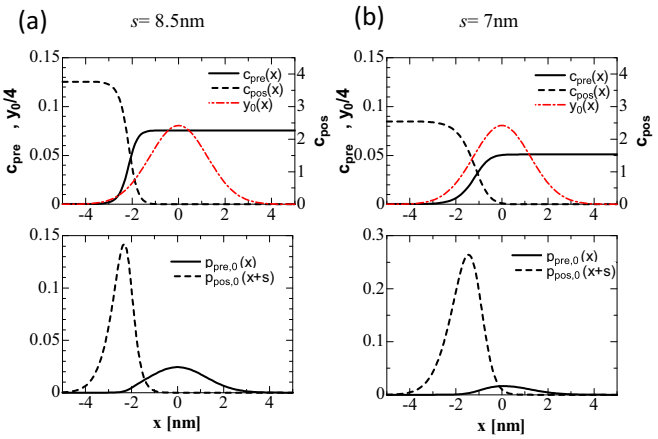

FIG. 3. The coefficients multiplied by y_0 (alternate short and long dashed lines) and the resultant stationary densities for XB_{preR} (solid lines) and XB_{postR} (broken lines) in the lower panels with working stroke sizes (a) $s = 8.5$ nm and (b) $s = 7$ nm (b). Here, $c_{pre}(x) = P_{pxb,0}av(x)/e(x)$ and $c_{pos}(x) = P_{pxb,0}af(x)/e(x)$. The parameters are given as $a = 500$, $d = 5000$, $g = 100$, $r_{xb} = 10^5$ (1/s), $E_{pre} = 0.7E_{ATP}$, $E_c = 1.1E_{pre}$, and $E_{pos} = 0$.

poststroke density $p_{pos,0}$. In the case of $s = 7$ nm [Fig. 3(b)], 45% of myosin molecules are in the poststroke state XB_{postR}, whereas only 4% are in the prestroke state XB_{preR}. In this case, the fluctuation between the pre- and poststroke states is quite small compared with the case of $s = 8.5$ nm.

In addition to the property of its kernel vector, the operator $\boldsymbol{A}$ has the following properties when the density functions are discretized by a finite number of intervals, and thereby the operator is represented by a finite-dimensional matrix. The diagonal components of $\boldsymbol{A}$ are positive and all the off-diagonals are nonpositive. Furthermore, the column sums of $\boldsymbol{A}$ are equal to zero. Thus, the transpose of $\boldsymbol{A}$ is a diagonally dominant matrix whose row sums are equal to zero. This also implies that the image of $\boldsymbol{A}$ is composed of the vectors whose component sum is equal to zero. From the Gershgorin circle theorem [20], we observe that the real parts of the nonzero eigenvalues of $\boldsymbol{A}$ other than the kernel vector are positive. The sums of the components of the eigenvectors of these nonzero eigenvalues are zero. Thus, the solution of Eq. (14) with fixed z values ($dz/dt = 0$) converges to $\boldsymbol{p}_0$ for any initial density whose integral is equal to 1. This also implies that $\boldsymbol{p}(t) \equiv \boldsymbol{p}_0$ with $z(t) \equiv z_0 = k_M \boldsymbol{B}\boldsymbol{p}_0/k_z$ satisfies Eqs. (14) and (15) simultaneously. Therefore, there is also a unique stationary solution for the coupled system. If the system provides an autonomous oscillation, this stationary solution must be unstable. Thus, we analyze the Jacobian matrix at this stationary solution to seek the conditions for the oscillations.

III. DERIVATION OF THE JACOBIAN MATRIX AT THE STATIONARY SOLUTION

To compute the Jacobian matrix at the stationary solution, we substitute dz/dt given in Eq. (15) into Eq. (14), which results in the following equivalent representation of the coupled system:

$$\begin{bmatrix} \frac{d\boldsymbol{p}}{dt}(t) \\ \frac{dz}{dt}(t) \end{bmatrix} = \begin{bmatrix} -\boldsymbol{A}\boldsymbol{p}(t) \\ 0 \end{bmatrix} + \frac{1}{\gamma}[k_M \boldsymbol{B}\boldsymbol{p}(t) - k_z z(t)] \begin{bmatrix} \boldsymbol{C}\boldsymbol{p}(t) \\ 1 \end{bmatrix}. \tag{32}$$

Equation (32) can be further deformed as the rank-1 update of the original state transition matrix as follows:

$$\begin{bmatrix} \frac{d\boldsymbol{p}}{dt}(t) \\ \frac{dz}{dt}(t) \end{bmatrix} = \left(\begin{bmatrix} -\boldsymbol{A} & \boldsymbol{0} \\ \boldsymbol{0} & 0 \end{bmatrix} + \frac{1}{\gamma} \begin{bmatrix} \boldsymbol{C}\boldsymbol{p}(t) \\ 1 \end{bmatrix} \otimes \begin{bmatrix} k_M \boldsymbol{B}^T \\ -k_Z \end{bmatrix} \right) \begin{bmatrix} \boldsymbol{p}(t) \\ z(t) \end{bmatrix}. \tag{33}$$

Here, the tensor product of two vectors $\boldsymbol{a}$ and $\boldsymbol{b}$ implies that $\boldsymbol{a} \otimes \boldsymbol{b} \equiv \boldsymbol{a}\boldsymbol{b}^T$. The rank-1 update term (the second term) on the right-hand side of Eq. (33) has the following mechanical meaning: The row vector on the right-hand side corresponds to the operator that measures the velocity deviation generated by the mechanical disequilibrium of current state $\boldsymbol{p}(t)$ and $z(t)$, while the column vector represents the shift of densities caused by the unit sliding speed.

From the fact that $k_M \boldsymbol{B}\boldsymbol{p}_0 - k_Z z_0 = 0$, the derivative of the right-hand side of Eq. (32) with respect to $\boldsymbol{p}$ and z at the stationary solution $\{\boldsymbol{p}_0, z_0\}$ is given as

$$\begin{aligned} &\boldsymbol{\delta} \begin{bmatrix} \frac{1}{\gamma}(k_M \boldsymbol{B}\boldsymbol{p} - k_z z)\boldsymbol{C}\boldsymbol{p} - \boldsymbol{A}\boldsymbol{p} \\ \frac{1}{\gamma}(k_M \boldsymbol{B}\boldsymbol{p} - k_z z) \end{bmatrix}_{\boldsymbol{p}_0, z_0} \\ &= \left(\begin{bmatrix} -\boldsymbol{A} & \boldsymbol{0} \\ \boldsymbol{0} & 0 \end{bmatrix} + \frac{1}{\gamma} \begin{bmatrix} \boldsymbol{C}\boldsymbol{p}_0 \\ 1 \end{bmatrix} \otimes \begin{bmatrix} k_M \boldsymbol{B}^T \\ -k_Z \end{bmatrix} \right) \begin{bmatrix} \boldsymbol{\delta}p \\ \delta z \end{bmatrix}. \end{aligned} \tag{34}$$

We refer to the coefficient matrix on the right-hand side of Eq. (34) as the Jacobian matrix $\boldsymbol{K}_0$. This matrix is regarded as the rank-1 update of the matrix that represents only the state transitions in the isometric contraction as follows:

$$\boldsymbol{K}_0 = \begin{bmatrix} -\boldsymbol{A} & \boldsymbol{0} \\ \boldsymbol{0} & 0 \end{bmatrix} + \frac{1}{\gamma} \begin{bmatrix} \boldsymbol{C}\boldsymbol{p}_0 \\ 1 \end{bmatrix} \otimes \begin{bmatrix} k_M \boldsymbol{B}^T \\ -k_Z \end{bmatrix}. \tag{35}$$

If a spontaneous oscillation is generated, there must be some eigenvalues with positive real parts in the Jacobian matrix $\boldsymbol{K}_0$. Because the matrix $-\boldsymbol{A}$ has a one-dimensional kernel and the real parts of its other eigenvalues are negative, the rank-1 update term changes this stability in oscillatory cases.

IV. ANALYSIS FOR CONDITIONS OF OSCILLATION USING THE JACOBIAN MATRIX

The condition of having eigenvalues with positive real parts can be identified based on the following theorem.

Theorem 1. A complex number λ with a positive real part is an eigenvalue of $\boldsymbol{K}_0$ if and only if the following equation holds:

$$\lambda k_M \boldsymbol{B}(\boldsymbol{A} + \lambda \boldsymbol{I})^{-1} \boldsymbol{C}\boldsymbol{p}_0 - \lambda\gamma - k_Z = 0. \tag{36}$$

Proof. From Eq. (35), we observe that $\begin{bmatrix} \boldsymbol{p}_\lambda \\ 1 \end{bmatrix}$ is the eigenvector of $\boldsymbol{K}_0$ with eigenvalue λ if and only if the following equations

hold:

$$(\boldsymbol{A}+\lambda\boldsymbol{I})\boldsymbol{p}_\lambda = \lambda\boldsymbol{C}\boldsymbol{p}_0, \tag{37}$$

$$\frac{1}{\gamma}(k_M\boldsymbol{B}\boldsymbol{p}_\lambda - k_Z) = \lambda. \tag{38}$$

From the assumption, $\boldsymbol{A}+\lambda\boldsymbol{I}$ is invertible. By substituting $\boldsymbol{p}_\lambda$ obtained from Eq. (37) into Eq. (38), we obtain Eq. (36). ■

We restrict our consideration to only the positive real eigenvalues instead of considering the right half-plane in the Gauss plane. We introduce a function that will be used to measure the potential of a spontaneous oscillation as

$$K(\lambda) \equiv \lambda k_M \boldsymbol{B}(\boldsymbol{A}+\lambda\boldsymbol{I})^{-1}\boldsymbol{C}\boldsymbol{p}_0 - \lambda\gamma, \quad \lambda > 0. \tag{39}$$

If the function $K(\lambda)$ is positive for a certain positive real number λ, then Eq. (36) is satisfied with $k_Z = K(\lambda) > 0$, and $\boldsymbol{p}_\lambda$ in Eq. (37) is the corresponding eigenvector. To analyze the property of the function $K(\lambda)$, we introduce the scaled eigenvector given by

$$\boldsymbol{q}_\lambda \equiv \frac{1}{\lambda}\boldsymbol{p}_\lambda = (\boldsymbol{A}+\lambda\boldsymbol{I})^{-1}\boldsymbol{C}\boldsymbol{p}_0, \quad \lambda > 0. \tag{40}$$

The densities in the pre- and poststroke states corresponding to $\boldsymbol{q}_\lambda$ can be explicitly represented by the rate constants as follows:

Theorem 2. Let $q_{\mathrm{pre},\lambda}$ and $q_{\mathrm{pos},\lambda}$ be the density functions corresponding to the pre- and poststroke components of $\boldsymbol{q}_\lambda$ in Eq. (40), respectively. Additionally, let $Q_{\mathrm{pxb},\lambda}$ be the scalar corresponding to the P_{XB} component of $\boldsymbol{q}_\lambda$. Then, the P_{XB} component is given by

$$Q_{\mathrm{pxb},\lambda} = -\frac{\int\left(\frac{f(x)+v(x)+\lambda}{h_\lambda(x)}\frac{dp_{\mathrm{pre},0}}{dx}(x) + \frac{b(x)+u(x)+\lambda}{h_\lambda(x)}\frac{dp_{\mathrm{pos},0}}{dx}(x+s)\right)dx}{1+a\int\frac{f(x)+v(x)+\lambda}{h_\lambda(x)}y_0(x)dx}, \tag{41}$$

and the density function parts are given by

$$q_{\mathrm{pre},\lambda}(x) = \frac{v(x)+\lambda}{h_\lambda(x)}\frac{dp_{\mathrm{pre},0}}{dx}(x) + \frac{b(x)}{h_\lambda(x)}\frac{dp_{\mathrm{pos},0}}{dx}(x+s) + aQ_{\mathrm{pxb},\lambda}\frac{v(x)+\lambda}{h_\lambda(x)}y_0(x), \tag{42}$$

$$q_{\mathrm{pos},\lambda}(x+s) = \frac{f(x)}{h_\lambda(x)}\frac{dp_{\mathrm{pre},0}}{dx}(x) + \frac{u(x)+\lambda}{h_\lambda(x)}\frac{dp_{\mathrm{pos},0}}{dx}(x+s) + aQ_{\mathrm{pxb},\lambda}\frac{f(x)}{h_\lambda(x)}y_0(x), \tag{43}$$

where the function h_λ is defined by

$$h_\lambda(x) = [u(x)+\lambda][v(x)+\lambda] - f(x)b(x). \tag{44}$$

The proof of this theorem is given by applying Eqs. (20)–(22), as shown in Appendix B.

From Eqs. (41)–(43), we observe that $\lim_{\lambda\to+\infty}\boldsymbol{B}(\boldsymbol{A}+\lambda\boldsymbol{I})^{-1}\boldsymbol{C}\boldsymbol{p}_0 = 0$, and $\boldsymbol{B}(\boldsymbol{A}+\lambda\boldsymbol{I})^{-1}\boldsymbol{C}\boldsymbol{p}_0$ converges to a finite value for $\lambda \to +0$. Thus, we observe that $K(\lambda) \approx -\gamma\lambda$ for sufficiently large λ, and $K(\lambda)$ converges to zero for $\lambda \to +0$. Therefore, if the maximum of K ($K_{\max}$) is positive, there are at least two real positive eigenvalues that fulfill Eq. (36) for a given $k_Z < K_{\max}$. To evaluate $K_{\max}$ for a realistic sarcomere model, we have to determine an appropriate value of the viscosity coefficient γ for the myofibrils. Because the equation of motion in Eq. (10) is given per one actin filament in the half-sarcomere, the corresponding macroscopic viscosity η is given by

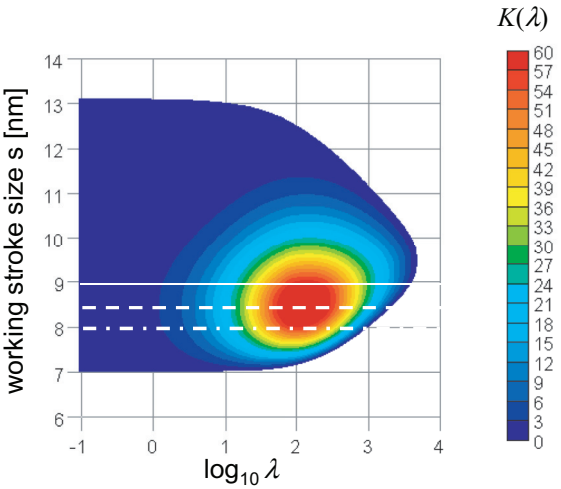

FIG. 4. The contour of function $K(\lambda)$ for various working stroke sizes s. Only the region where K takes a positive value is contoured. The typical working stroke size ($s = 8.5$ nm) is indicated by the dashed line. The other lines indicate $s = 9$ nm (solid) and $s = 8$ nm (alternate long and short dashed line). The parameters are given as $a = 500, d = 5000, g = 100, r_{\mathrm{xb}} = 10^5$ (1/s), $E_{\mathrm{pre}} = 0.7E_{\mathrm{ATP}}$, $E_c = 1.1E_{\mathrm{pre}}$, and $E_{\mathrm{pos}} = 0$. The spring constant of the myosin arm is $k_M = 2.8$ pN/nm and the viscosity per one actin filament is $\gamma = 10^{-5}$ pN s/nm.

$$\eta\ (\mathrm{N\,s/m^2}) = \frac{\gamma\ (\mathrm{pN\,s/nm})10^{-12}\ (\mathrm{N/pN})\frac{SL_0}{2}\ (\mathrm{nm})}{SA_0\ (\mathrm{nm^2})10^{-18}\ (\mathrm{m^2/nm^2})} \approx 10^6\gamma\ (\mathrm{pN\,s/nm}). \tag{45}$$

We inserted $SL_0/2 = 10^3$ nm as the half-sarcomere length, and $SA_0 = 10^3$ nm^2 as the cross-sectional area per one actin filament. In this paper, we apply the macroscopic value $\eta = 10$ N s/m^2 [21]. This corresponds to the microscopic value $\gamma = 10^{-5}$ pN s/nm.

In Fig. 4, the contour of $K(\lambda)$ is shown for working stroke size s from 6 to 14 nm, where only the positive region of K is contoured, and the logarithmic scale is applied for λ. Here, K is evaluated by numerically integrating the functions given in Eqs. (42) and (43). If the horizontal line corresponding to the given working stroke size s intersects with the contoured region, at least the half-sarcomere system shows oscillatory behavior for sarcomere stiffness k_Z smaller than the maximum of $K(\lambda)$ on the horizontal line. The landscape of K indicates that there are two positive eigenvalues for a given k_Z. The smaller positive eigenvalue increases and the larger eigenvalue decreases as sarcomere stiffness k_Z increases. The increase of the smaller positive eigenvalue is also observed for the change of the working stroke size s. That is, the smaller positive eigenvalue increases as the working stroke size increases from $s = 8.5$ nm for fixed sarcomere stiffness k_Z. Because

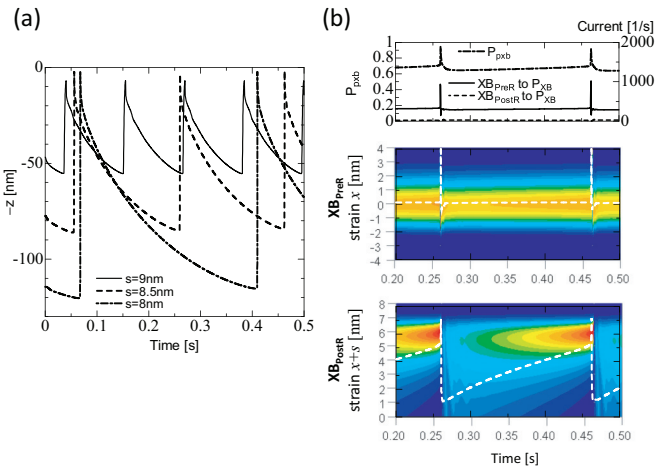

FIG. 5. The oscillatory behavior. (a) The time courses of $-z$ for the working stroke sizes $s = 8$, 8.5, and 9 nm. (b) The contours of densities $p_{\rm pre}$ (top panel) and $p_{\rm pos}$ (bottom panel) for the pre- and poststroke states, respectively (b) in the case of $s = 8.5$ nm. The averaged strains are drawn with white broken lines. The time courses of $P_{\rm pxb}$ and the currents of the detachments from $\rm XB_{preR}$ and $\rm XB_{postR}$ are shown in the top panel. The parameters related to the rate constants are given as $a = 500$, $d = 5000$, $g = 100$, $r_{\rm xb} = 10^5$ (1/s), $E_{\rm pre} = 0.7E_{\rm ATP}$, $E_c = 1.1E_{\rm pre}$, and $E_{\rm pos} = 0$. The spring constant of the myosin arm is $k_M = 2.8$ pN/nm, and the viscosity per one actin filament is $\gamma = 10^{-5}$ pN s/nm. These numerical results were obtained by applying the explicit Euler scheme.

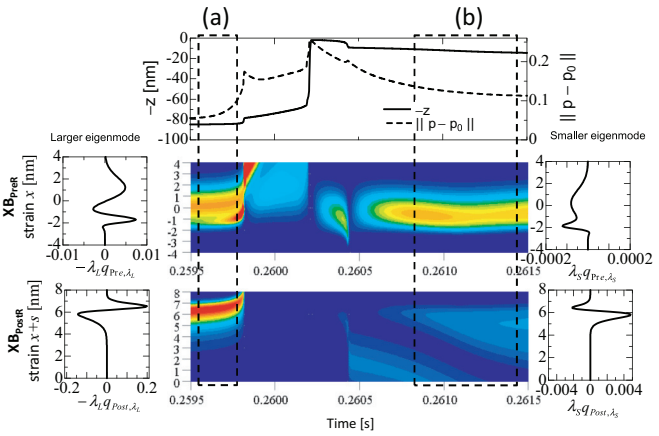

FIG. 6. The enlarged views of the density contours in the time interval [0.2595,0.2615] around the rapid stretching area in the case of $s = 8.5$ nm. The time courses of the $-z$ value (top panel: solid line) and the distance from the stationary density (top panel: broken line) are shown together with the contours of the densities $p_{\rm pre}$ (middle panel) and $p_{\rm pos}$ (bottom panel). These numerical results were obtained by applying the explicit Euler scheme. The regions surrounded by the broken lines correspond to the turning points approaching and leaving the stationary solution by the larger positive eigenmode (left) and the smaller positive eigenmode (right), respectively. These eigenmodes were obtained analytically from Eqs. (42) and (43). The parameters related to the rate constants are given as $a = 500$, $d = 5000$, $g = 100$, $r_{\rm xb} = 10^5$ (1/s), $E_{\rm pre} = 0.7E_{\rm ATP}$, $E_c = 1.1E_{\rm pre}$, and $E_{\rm pos} = 0$. The spring constant of the myosin arm is $k_M = 2.8$ pN/nm and the viscosity per one actin filament is $\gamma = 10^{-5}$ pN s/nm.

parameter k_Z indicates the spring constant per one actin filament in the half-sarcomere, the following equation defines the relationship with the macroscopic Young's modulus E of the myofibril fiber:

$$E\ (\mathrm{N/m^2}) = \frac{k_Z\ (\mathrm{pN/nm})10^{-12}\ (\mathrm{N/pN})\frac{SL_0}{2}\ (\mathrm{nm})}{SA_0\ (\mathrm{nm^2})10^{-18}\ (\mathrm{m^2/nm^2})}$$
$$\approx 10^6 k_Z\ (\mathrm{pN/nm}). \quad (46)$$

Because De Winkel *et al.* [24] estimated Young's modulus of the skeletal muscle fiber in a relaxed state as approximately $E = 3 \times 10^6$ N/m^2, we apply $k_Z = 3$ pN/nm. In Fig. 5(a), the time courses of $-z$ obtained by the numerical time integrations are shown for the three working strong sizes around $s = 8.5$ nm, which is close to the value experimentally estimated by Kaya *et al.* [14]. Shintani *et al.* [3] observed 5–10 % of the total sarcomere length as the amplitude with 7–9 Hz frequency for the rat neonatal cardiomyocytes. Because the half-sarcomere length is approximately 1000 nm, the oscillation produced by our numerical model with the working stroke size around $s = 8.5$ nm reproduced this experimental phenomenon well, as shown in Fig. 5(a). For these three cases, the smaller positive eigenvalues are 3.7, 3.5, and 4.4 (1/s) for the working stroke sizes $s = 8$, 8.5, and 9 (nm), respectively, whereas the larger positive eigenvalues are 1310, 3172, and 5910 (1/s), respectively. Because the eigenvalue of $\boldsymbol{K}_0$ corresponds to the value of $(dz/dt)/(z - z0)$ according to the last row in Eq. (33), its magnitude represents the strain rates. Therefore, the smaller positive eigenmode may induce the slow decline of $-z$ (slow shortening of the sarcomere), whereas the larger positive eigenmode may induce the fast rise of $-z$ (quick lengthening of the sarcomere). In Fig. 5(b), the contours of the time course of the densities obtained by the numerical time integrations for the pre- and poststroke states are shown in the case of $s = 8.5$ nm. The steep rise of the $-z$ value that corresponds to the rapid stretching of the sarcomere is caused by the collective reversal strokes from $\rm XB_{postR}$. As shown by the broken line for $\rm XB_{postR}$, the sudden increase of the average strain is observed at the beginning of the collective disappearance from the poststroke state. Once the sarcomere starts to stretch after achieving its maximal contraction force, the chain reaction of the reversal strokes is induced. Because a relatively large detachment rate constant [$d = 5000$ (1/s)] is provided from $\rm XB_{preR}$ compared with the attachment rate constant [$a = 500$ (1/s)] to $\rm XB_{preR}$ and the detachment rate constant [$g = 100$ (1/s)] from $\rm XB_{postR}$, the collective reversal strokes result in the collective detachments through $\rm XB_{preR}$. This is clearly observed in the peaks of the detachment current from $\rm XB_{preR}$ to $\rm P_{XB}$ shown in the top panel of Fig. 5(b).

To view more details around the rapid stretching area, the enlarged images of the density contours are shown with the positive eigenmodes on both sides in Fig. 6. We can observe that these eigenmodes capture the changes of densities in the time intervals surrounded by the broken lines well, where the density approaches the stationary density and leaves it. The distance between the obtained density $\boldsymbol{p}$ and the stationary

density $\boldsymbol{p}_0$ is measured as follows:

$$\|\boldsymbol{p}-\boldsymbol{p}_0\|^2=(P_{\rm pxb}-P_{\rm pxb,0})^2+\int(p_{\rm pre}-p_{\rm pre,0})^2dx + \int(p_{\rm pos}-p_{\rm pos,0})^2dx. \quad (47)$$

Regarding the larger positive eigenvalue λ_L, the eigenmodes shown in the figure result from multiplying the original eigenmodes given in Eqs. (42) and (43) by -1, whose z components are 1 because the z value is decreasing in the time interval in the broken line (a). The progress of the contours in the broken line (a) match the profiles of the eigenmodes shown on the left well. Thus, the larger eigenmodes form unstable densities before rapid stretching. Conversely, the progress of the contours in the time interval surrounded by broken line (b) are more consistent with the smaller eigenmodes shown on the right. Therefore, the smaller eigenmodes seem to induce contractions of the sarcomere that are much slower than stretching.

V. FACTORS DETERMINING OSCILLATORY BEHAVIOR

It is not a simple task to provide physical interpretations of the contributions of the three terms in Eqs. (42) and (43) regarding making the function K positive. However, it may be important to evaluate the significance of the contributions of these terms. The first two terms come from the spatial derivative of the stationary densities; thus, they are related somehow to the density shift caused by filament sliding. We analyze the contributions of these three terms by decomposing K into six terms according to Eqs. (42) and (43):

$$K = K_{{\rm pre},d{\rm pre}}+K_{{\rm pre},d{\rm pos}}+K_{{\rm pre},y0}+K_{{\rm pos},d{\rm pre}} + K_{{\rm pos},d{\rm pos}}+K_{{\rm pos},y0}-\gamma\lambda, \quad (48)$$

with

$$K_{{\rm pre},d{\rm pre}}(\lambda)\equiv\lambda k_M\int x\frac{v(x)+\lambda}{h_\lambda(x)}\frac{dp_{\rm pre,0}}{dx}(x)dx,$$

$$K_{{\rm pre},d{\rm pos}}(\lambda)\equiv\lambda k_M\int x\frac{b(x)}{h_\lambda(x)}\frac{dp_{\rm pos,0}}{dx}(x+s)dx,$$

$$K_{{\rm pre},y0}(\lambda)\equiv\lambda k_M a Q_{\rm pxb}\int x\frac{v(x)+\lambda}{h_\lambda(x)}y_0(x)dx,$$

$$K_{{\rm pos},d{\rm pre}}(\lambda)\equiv\lambda k_M\int(x+s)\frac{f(x)}{h_\lambda(x)}\frac{dp_{\rm pre,0}}{dx}(x)dx,$$

$$K_{{\rm pos},d{\rm pos}}(\lambda)\equiv\lambda k_M\int(x+s)\frac{u(x)+\lambda}{h_\lambda(x)}\frac{dp_{\rm pos,0}}{dx}(x+s)dx,$$

$$K_{{\rm pos},y0}(\lambda)\equiv\lambda k_M a Q_{\rm pxb}\int(x+s)\frac{f(x)}{h_\lambda(x)}y_0(x)dx.$$

In Table I, the above six components are evaluated for the two positive eigenvalues that fulfill $K(\lambda)=k_Z=3$ pN/nm in the cases of the three working stroke sizes $s=8$, 8.5, and 9 nm. For the smaller eigenvalues, the contribution of $K_{{\rm pos},d{\rm pos}}$ is always significant. For the comparison with the nonoscillatory case of working stroke size $s=7$ nm, the six components for λ corresponding to the smaller eigenvalue in the case of $s=8.5$ nm are shown in the last column. In this case, although $K_{{\rm pos},d{\rm pos}}$ is of the same magnitude as in the case of $s=8.5$ nm, the strong negative value of $K_{{\rm pos},y0}$ makes the sum less than zero. Note that the values of $Q_{\rm pxb}$ are $-7.0e-4$ for $s=8.5$ nm and $-5.3e-4$ for $s=7$ nm. Thus, the large difference between these two cases comes from the coefficient function f/h_λ on $[-2,0]$, as shown in Fig. 3 for $\lambda=0$. The term $K_{{\rm pos},y0}$ corresponds to the contribution of the transition from P_{XB} to XB_{postR} through XB_{preR}. If this transition is energetically too easy, the negative contribution of this term on K prevents the oscillation.

TABLE I. The six components of the function $K(\lambda)$. For the working stroke sizes $s=8$, 8.5, and 9 nm, the component values at the positive two eigenvalues that fulfill $K(\lambda)=k_Z=3$ pN/nm are shown. The case of $s=7$ nm is also shown for comparison with $s=8.5$ nm. The terms that make the most significant contribution are underlined. The parameters related to the rate constants are given as $a=500$, $d=5000$, $g=100$, $r_{\rm xb}=10^5$ (1/s), $E_{\rm pre}=0.7E_{\rm ATP}$, $E_c=1.1E_{\rm pre}$, and $E_{\rm pos}=0$. The spring constant of the myosin arm is $k_M=2.8$ pN/nm and the viscosity per one actin filament is $\gamma=10^{-5}$ pN s/nm.

		$K_{{\rm pre},*}$ (pN/nm)			$K_{{\rm pos},*}$ (pN/nm)		
s (nm)	λ (1/s)	$d$pre	$d$pos	$y0$	$d$pre	$d$pos	$y0$
8	3.66	−0.008	0.026	−0.011	0.23	<u>4.19</u>	−1.43
	1310	−2.31	1.95	−0.105	<u>9.61</u>	−4.67	−1.47
8.5	3.48	−0.010	0.025	−0.006	0.17	<u>3.55</u>	−0.73
	3172	−5.10	2.95	−0.035	<u>9.64</u>	−4.16	−0.26
9	4.40	−0.014	0.026	−0.003	0.15	<u>3.21</u>	−0.37
	5910	−8.17	3.25	−0.010	<u>8.24</u>	−0.20	−0.05
7	3.48	−0.005	0.008	−0.012	0.25	1.64	<u>−1.87</u>

To observe how the positive values are determined for $K_{{\rm pos},d{\rm pre}}(\lambda)$ and $K_{{\rm pos},d{\rm pos}}(\lambda)$, which make significant contributions to the larger and smaller positive eigenvalues, respectively, we show their coefficient functions $\lambda f(x)/h_\lambda(x)$ and $\lambda[u(x)+\lambda]/h_\lambda(x)$, and the derivatives $dp_{\rm pre,0}/dx$ and $dp_{\rm pos,0}/dx$ separately, with their products in Fig. 7 in the case of $s=8.5$ nm. Regarding $K_{{\rm pos},d{\rm pre}}(\lambda)$, most of the positive part of $dp_{\rm pre,0}/dx$ is cut off by the coefficient function $\lambda f(x)/h_\lambda(x)$ for smaller λ. However, this cutoff is relaxed as λ increases. Regarding $K_{{\rm pos},d{\rm pos}}(\lambda)$, the negative part of $dp_{\rm pos,0}/dx$ is cut off by the coefficient function for smaller λ. This makes the resultant product nearly a positive function. However, this cutoff is weakened as λ increases. In this way, the significance of the contribution changes according to the magnitude of λ.

VI. BALANCE OF DETACHMENT RATE CONSTANTS AT THE PRE- AND POSTSTROKE STATES

Thus far, we have studied three-state models in which the detachment rate constant at the prestroke state is much larger than that at the poststroke state. The magnitude of these rate constants and the balance between them do not conflict with the experimental observation made by Capitanio *et al.* [22]. By contrast, Erdmann *et al.* [23] applied a similar three-state model to each molecular motor in a small ensemble, in which the detachment rate constant d at XB_{preR} is set to 2 (1/s), which is much smaller than our value 5000 (1/s), and the detachment rate constant g at XB_{postR} is given by a

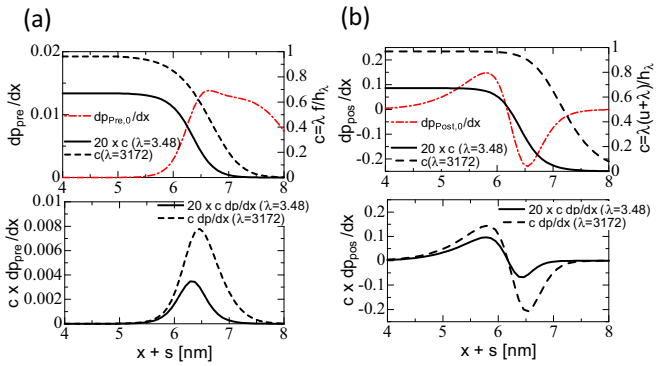

FIG. 7. The derivative $dp_{\mathrm{pre},0}/dx$ and $\lambda f/h_\lambda$ (a, top panel) and their products (a, bottom panel) for the smaller and larger positive eigenvalues, and the derivative $dp_{\mathrm{pos},0}/dx$ and $\lambda(u+\lambda)/h_\lambda$ (b, top panel) and their products (b, bottom panel) for the smaller (solid line) and larger (broken line) positive eigenvalues. The parameters related to the rate constants are given as $a = 500$, $d = 5000$, $g = 100$, $r_{\mathrm{xb}} = 10^5$ (1/s), $E_{\mathrm{pre}} = 0.7E_{\mathrm{ATP}}$, $E_c = 1.1E_{\mathrm{pre}}$, and $E_{\mathrm{pos}} = 0$. The spring constant of the myosin arm is $k_M = 2.8$ pN/nm and the viscosity per one actin filament is $\gamma = 10^{-5}$ pN s/nm.

load-dependent function:

$$\tilde{g}(x) = k_{20}^0 \exp[-kM(x+s)/F_0], \tag{49}$$

with $k_{20}^0 = 80$ (1/s) and $F_0 = 12.6$ pN. This definition of the rate constant prevents the detachment for the myosins that produce a positive contraction force and facilitates the detachment for the myosins that produce a negative force. Therefore, the efficiency is improved by applying this type of load-dependent detachment rate. Because Erdmann *et al.* adopted the so-called parallel cluster model (PCM), in which all molecular motors in the same state have a common strain in their elastic elements, the ensemble is different from our sarcomere model. Therefore, we cannot expect similar behavior. Nevertheless, it may be interesting to observe what happens in our model when a parameter set similar to their model is applied. Because their original value of d is too small to produce oscillations with our sarcomere model, we adopted $d = 20$ (1/s). The results are shown in Fig. 8. For comparison, the results obtained by resetting a and d to our original values are shown in the insets. In our model, when a is smaller than k_{20}^0, the quick contractions [the sharp fall of $-z$ in Fig. 8(a)] trigger oscillations. These quick contractions are produced by the collective power strokes, and these forward transitions are clearly captured by the eigenmode of the larger positive eigenvalue λ_L (=3873) shown in Fig. 8(b). Unlike the case with the original rate constants at $\mathrm{XB_{preR}}$ shown in the inset, a prominent change is observed for the components of $\mathrm{XB_{preR}}$ (the broken lines). This can be explained by considering Eq. (42) because the coefficient of $dp_{\mathrm{pre},0}/dx$ increases with the decrease of d. By contrast, the change at $\mathrm{XB_{preR}}$ is inconspicuous in the original case because of the fast detachment. Regarding the original rate constant case at $\mathrm{XB_{preR}}$, although the time course of $-z$ changes with the introduction of the load-dependent detachment rate, the basic mechanism of the oscillation in the power-stroke model is the same; that is, the oscillation is triggered by quick relaxation due to the collective reversal strokes.

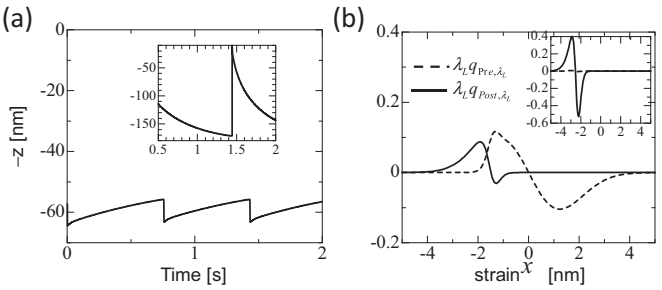

FIG. 8. Oscillatory behavior for the small detachment rate constant $d = 20$ from $\mathrm{XB_{preR}}$, where the force-dependent detachment rate g from $\mathrm{XB_{postR}}$ is adopted. (a) The time courses of $-z$. (b) The eigenmode $\boldsymbol{p}_\lambda = \lambda q_\lambda$ for the larger positive eigenvalue $\lambda_L = 3659$. The other parameters are given as $a = 40$, $r_{\mathrm{xb}} = 10^5$ (1/s), $E_{\mathrm{pre}} = 0.7E_{\mathrm{ATP}}$, $E_c = 1.1E_{\mathrm{pre}}$, and $E_{\mathrm{pos}} = 0$. The spring constant of the myosin arm is $k_M = 2.8$ pN/nm and the viscosity per one actin filament is $\gamma = 10^{-5}$ pN s/nm. For comparison, the results, where only a and d are reset to the original values ($a = 500$, $d = 5000$), are shown in the insets.

VII. RELEVANCE OF HOPF BIFURCATION

Previous studies [10–12] that analyzed the two-state model interpreted the onset of spontaneous oscillations as Hopf bifurcation, in which a pair of complex-conjugate eigenvalues cross the imaginary axis, and the frequency of the oscillations to linear order is given by the magnitude of the imaginary part

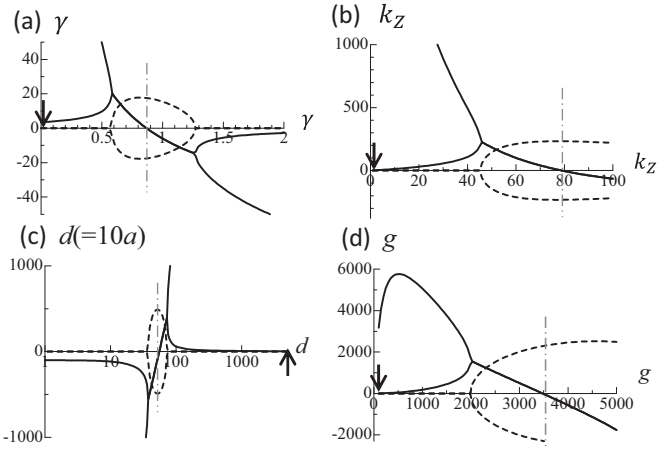

FIG. 9. The eigenvalue perturbations from the two real positive eigenvalues. The real and imaginary parts of the eigenvalues are shown by the solid and broken lines, respectively. (a) The viscosity coefficient γ is perturbed from 10^{-5} to 2 pN s/nm. (b) The spring constant k_Z per one actin filament for the sarcomeric stiffness is perturbed from 1 to 100 pN/nm. (c) The detachment rate constant d from $\mathrm{P_{XB}}$ is perturbed from 5000 to 1 (1/s), where the attachment rate constant to $\mathrm{P_{XB}}$ is given as $a = 0.1d$. The logarithmic scale is applied for d. (d) The detachment rate constant g from $\mathrm{XB_{postR}}$ is perturbed from 100 to 5000 (1/s). The parameters other than the perturbed parameter are given as $a = 500$, $d = 5000$, $g = 100$, $r_{\mathrm{xb}} = 10^5$ (1/s), $E_{\mathrm{pre}} = 0.7E_{\mathrm{ATP}}$, $E_c = 1.1E_{\mathrm{pre}}$, $E_{\mathrm{pos}} = 0$, $k_M = 2.8$ pN/nm, and $\gamma = 10^{-5}$ pN s/nm. The vertical alternating long and dashed lines indicate the onset of Hopf bifurcations. The arrows indicate the parameter values adopted in our model.

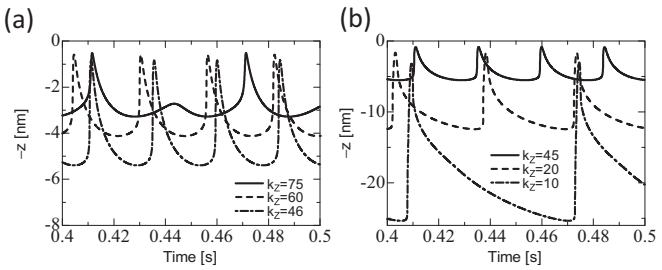

FIG. 10. The change of time courses of $-z$ for the various sarcomeric stiffness k_Z (a) from the onset of Hopf bifurcation to the merge point to one real eigenvalue, and (b) after branching into two real eigenvalues.

of these eigenvalues. However, in our case, we have observed that there are two real positive eigenvalues, where the larger eigenvalue is associated with quick relaxation and the smaller eigenvalue is associated with slow contraction. To illustrate this difference, we perform a perturbation analysis of the eigenvalues with respect to the primal physical parameters, as shown in Fig. 9. These results indicate that the onset of instability is actually Hopf bifurcation in our case as well. However, our system provides the oscillation in the parameter region at a great distance from the onset. In this region, the pair of two conjugate eigenvalues starting from the onset merge into a real positive eigenvalue, and then the two eigenvalues branch into the real axis (zero imaginary part) as they approach our parameter region. In this analysis, all the eigenvalues of the discretized Jacobian in Eq. (35) are computed by applying the LAPACK eigenvalue routine DGEEV [25], and the nearest eigenvalues to those in the previous step are selected during the perturbation process. In all the cases, there are no other eigenvalues in the right half-plane other than those that are plotted.

We observe how the wave form (time course of $-z$) changes from the onset of Hopf bifurcation to the branching of the two real positive eigenvalues for one case. Figure 10 shows the change of wave form for the perturbation of sarcomeric stiffness k_Z. As stiffness k_Z decreases from the onset to the merge point, the rise of $-z$ gradually becomes sharper than the fall. Additionally, this change is accompanied by an increase of the amplitude [Fig. 10(a)]. After the merge into one real eigenvalue, the rise becomes even sharper with the rapid increase of the larger positive eigenvalue [Fig. 10(b)]. Additionally, the frequency decreases with the decrease of the smaller eigenvalue.

VIII. CONCLUSION

In this paper, the coupling of the state transitions of a molecular motor and sarcomeric movement was represented as the rank-1 update of the state transition matrix that corresponds to the isometric contraction. Based on this representation, the oscillatory behaviors of the three-state power-stroke model were analyzed using eigenmode analysis of the Jacobian matrix given by linearization at the stationary solution. We derived the condition (Theorem 1) that must be fulfilled by the eigenvalues of the Jacobian matrix. The observations made regarding the analytical representation of the eigenmodes (Theorem 2) and the criterion given by function K demonstrated the essence of the oscillations generated by the balance between the rate constants of the power stroke and the reversal stroke. The analysis through function K suggested that there were two eigenmodes of the Jacobian matrix that induced oscillatory behavior. The oscillations with physical parameters in the physiological ranges seem to be given by two eigenmodes with real positive eigenvalues, which are situated far away from a pair of conjugate imaginary eigenvalues that correspond to the onset of Hopf bifurcation. The magnitude of the smaller positive eigenvalue seems to be strongly related to the frequency of the oscillation, whereas the larger positive eigenmode seems to induce an unstable density before rapidly stretching with the collective reversal strokes that nearly cause the population to disappear in the poststroke state.

Because our study is based on linearization at the stationary solution, our analysis is effectively limited to the description of instabilities for small deviations from the stationary solution; that is, we cannot explain the regular periodicity with current theory. Thus, a more complete understanding of the oscillatory behavior may require more advanced approaches beyond linearization. Several details of the actual system are simplified in our three-state model. Our model does not cover all the known molecular states in the actomyosin ATPase cycle [26]. The three-dimensional geometry of the sarcomere (overlaps of the two filaments, the positions of the binding sites along the actin filament, and the myosin heads along the myosin filament) are not taken into account. Thus, we have to refine our model from this point of view in our future work.

ACKNOWLEDGMENTS

T.W. and T.H.'s work was supported in part by the Ministry of Education, Culture, Sports, Science and Technology of Japan (MEXT) as Strategic Programs for Innovative Research Field 1 Supercomputational Life Science, and a social and scientific priority issue (Integrated computational life science to support personalized and preventive medicine) to be analyzed using the post-K computer. S.A.S. and H.H.'s work was supported by Grants-in-Aid for Scientific Research on Innovative Areas (H.H. 23107002), for Research Fellow (S.A.S. 15J07373), and for Scientific Research (B) (H.H. 16H04773) from the Japan Society for the Promotion of Science.

APPENDIX A: COMPUTATION OF THE KERNEL VECTOR OF A

Once $P_{\mathrm{pxb},0}$ is determined, the density functions are given as

$$\begin{aligned}\begin{bmatrix}\{\hat{p}_{\mathrm{pre},0}\}\\ \{\hat{p}_{\mathrm{pos},0}\}\end{bmatrix} &= \begin{bmatrix}\langle u\rangle & -\langle b\rangle\\ -\langle f\rangle & \langle v\rangle\end{bmatrix}^{-1}\begin{bmatrix}a P_{\mathrm{pxb},0}\{y_0\}\\ 0\end{bmatrix}\\ &= \begin{bmatrix}\langle v/e\rangle & \langle b/e\rangle\\ \langle f/e\rangle & \langle u/e\rangle\end{bmatrix}\begin{bmatrix}a P_{\mathrm{pxb},0}\{y_0\}\\ 0\end{bmatrix}\\ &= a P_{\mathrm{pxb},0}\begin{bmatrix}\langle v/e\rangle\{y_0\}\\ \langle f/e\rangle\{y_0\}\end{bmatrix}. \end{aligned} \tag{A1}$$

Because $\boldsymbol{p}_0$ is normalized, we have

$$a P_{\mathrm{pxb},0} \int \frac{[v(x)+f(x)]y_0(x)}{e(x)}dx + P_{\mathrm{pxb},0} = 1. \tag{A2}$$

This determines $P_{\mathrm{pxb},0}$. Because the 2×2 matrix in Eq. (A1) is regular, it is obvious that the kernel of $\boldsymbol{A}$ is one-dimensional space spanned by $\boldsymbol{p}_0$.

APPENDIX B: COMPUTATION OF THE EIGENMODE

The proof of Theorem 2 is based on the following formula that provides the inverse of an arbitrary block 2×2 matrix:

$$\begin{bmatrix}\alpha & \beta\\ \gamma & \omega\end{bmatrix}^{-1} = \begin{bmatrix}\alpha^{-1}+\alpha^{-1}\beta\sigma^{-1}\gamma\alpha^{-1} & -\alpha^{-1}\beta\sigma^{-1}\\ -\sigma^{-1}\gamma\alpha^{-1} & \sigma^{-1}\end{bmatrix}, \tag{B1}$$

where σ is the Schur complement matrix given by

$$\sigma = \omega - \gamma\alpha^{-1}\beta. \tag{B2}$$

We apply Eq. (B1) to the following matrix:

$$\boldsymbol{A}+\lambda\boldsymbol{I} = \begin{bmatrix}\langle u+\lambda\rangle & -\langle b\rangle & -a\{y_0\}\\ -\langle f\rangle & \langle v+\lambda\rangle & \{0\}\\ -\{d\}^T & -\{g\}^T & a+\lambda\end{bmatrix} \tag{B3}$$

with

$$\alpha = \begin{bmatrix}\langle\hat{u}\rangle & -\langle b\rangle\\ -\langle f\rangle & \langle\hat{v}\rangle\end{bmatrix},\quad \beta = \begin{bmatrix}-a\{y_0\}\\ \{0\}\end{bmatrix},$$
$$\gamma = [-\{d\}-\{g\}],\quad \omega = a+\lambda,$$

where $\hat{u} = u+\lambda$ and $\hat{v} = v+\lambda$. By substituting the inverse of α given by

$$\alpha^{-1} = \begin{bmatrix}\langle\hat{v}/h_\lambda\rangle & \langle b/h_\lambda\rangle\\ \langle f/h_\lambda\rangle & \langle\hat{u}/h_\lambda\rangle\end{bmatrix} \tag{B4}$$

into Eqs. (B1) and (B2), we obtain

$$(\boldsymbol{A}+\lambda\boldsymbol{I})^{-1} = \begin{bmatrix}\tilde{\alpha} & \tilde{\beta}\\ \tilde{\gamma} & \tilde{\omega}\end{bmatrix} \tag{B5}$$

with

$$\tilde{\alpha} = \begin{bmatrix}\left\langle\frac{\hat{v}}{h_\lambda}\right\rangle & \left\langle\frac{b}{h_\lambda}\right\rangle\\ \left\langle\frac{f}{h_\lambda}\right\rangle & \left\langle\frac{\hat{u}}{h_\lambda}\right\rangle\end{bmatrix}$$
$$+a\sigma^{-1}\begin{bmatrix}\left\langle\frac{\hat{v}}{h_\lambda}\right\rangle\{y_0\}\left\{\frac{d\hat{v}+gf}{h_\lambda}\right\}^T & \left\langle\frac{\hat{v}}{h_\lambda}\right\rangle\{y_0\}\left\{\frac{db+g\hat{u}}{h_\lambda}\right\}^T\\ \left\langle\frac{f}{h_\lambda}\right\rangle\{y_0\}\left\{\frac{d\hat{v}+gf}{h_\lambda}\right\}^T & \left\langle\frac{f}{h_\lambda}\right\rangle\{y_0\}\left\{\frac{db+g\hat{u}}{h_\lambda}\right\}^T\end{bmatrix},$$

$$\tilde{\beta} = a\sigma^{-1}\begin{bmatrix}\left\{\frac{\hat{v}}{h_\lambda}y_0\right\}\\ \left\{\frac{f}{h_\lambda}y_0\right\}\end{bmatrix},$$

$$\tilde{\gamma} = \sigma^{-1}\begin{bmatrix}\left\{\frac{d\hat{v}+gf}{h_\lambda}\right\}^T & \left\{\frac{db+g\hat{u}}{h_\lambda}\right\}^T\end{bmatrix},$$

$$\tilde{\omega} = \sigma^{-1},$$

where the Schur complement is given by

$$\sigma = a+\lambda-a\left\{\frac{d\hat{v}+gf}{h_\lambda}\right\}^T\{y_0\}. \tag{B6}$$

From the fact that

$$\{1\}^T\{y_0\} = \int y_0(x)dx = 1, \tag{B7}$$

and the equality

$$d\hat{v}+gf-h_\lambda = -\lambda(f+\hat{v}), \tag{B8}$$

the Schur complement in Eq. (B6) can be further deformed as

$$\begin{aligned}\sigma &= \lambda - a\left\{\frac{d\hat{v}+gf}{h_\lambda}-1\right\}^T\{y_0\}\\ &= \lambda - a\{1\}^T\left\langle\frac{d\hat{v}+gf-h_\lambda}{h_\lambda}\right\rangle\{y_0\}\\ &= \lambda\left(1+a\left\{\frac{f+\hat{v}}{h_\lambda}\right\}^T\{y_0\}\right).\end{aligned} \tag{B9}$$

From the equality

$$db+g\hat{u}-h_\lambda = -\lambda(b+\hat{u}) \tag{B10}$$

and Eqs. (B7) and (B8), we also obtain

$$\frac{1}{\lambda}\{y_0\}\left\{\frac{d\hat{v}+gf}{h_\lambda}-1\right\}^T = -\{y_0\}\left\{\frac{f+\hat{v}}{h_\lambda}\right\}, \tag{B11}$$
$$\frac{1}{\lambda}\{y_0\}\left\{\frac{db+g\hat{u}}{h_\lambda}-1\right\}^T = -\{y_0\}\left\{\frac{b+\hat{u}}{h_\lambda}\right\}. \tag{B12}$$

Therefore, for operator $\{y\}$ corresponding to any function y whose integral is equal to zero,

$$\{1\}^T\{y\} = 0, \tag{B13}$$

we have

$$\begin{aligned}\sigma^{-1}\{y_0\}\left\{\frac{d\hat{v}+gf}{h_\lambda}\right\}^T\{y\} &= -\frac{\{y_0\}\{(f+\hat{v})/h_\lambda\}^T\{y\}}{1+a\{(f+\hat{v})/h_\lambda\}^T\{y_0\}}\\ &= -\frac{\int\frac{f+\hat{v}}{h_\lambda}y\,dx}{1+a\int\frac{f+\hat{v}}{h_\lambda}y_0dx}\{y_0\},\end{aligned} \tag{B14}$$
$$\begin{aligned}\sigma^{-1}\{y_0\}\left\{\frac{db+g\hat{u}}{h_\lambda}\right\}^T\{y\} &= -\frac{\{y_0\}\{(b+\hat{u})/h_\lambda\}^T\{y\}}{1+a\{(f+\hat{v})/h_\lambda\}^T\{y_0\}}\\ &= -\frac{\int\frac{b+\hat{u}}{h_\lambda}y\,dx}{1+a\int\frac{f+\hat{v}}{h_\lambda}y_0dx}\{y_0\}.\end{aligned} \tag{B15}$$

The derivatives $dp_{\mathrm{pre},0}/dx$ and $dp_{\mathrm{pos},0}/dx$ fulfill Eq. (B13). Thus, by applying Eqs. (B14) and (B15) in the multiplication of $\tilde{\alpha}$ to these derivatives, we obtain Theorem 2.

[1] J. W. Pringle, Proc. R. Soc. B **201**, 107 (1978).
[2] S. Ishiwata, Y. Shimamoto and N. Fukuda, Prog. Biophys. Mol. Biol. **105**, 187 (2011).
[3] S. A. Shintani, K. Oyama, N. Fukuda, and S. Ishiwata, Biochem. Biophys. Res. Commun. **457**, 165 (2015).
[4] T. Washio, K. Yoneda, J. Okada, T. Kariya, S. Sugiura, and T. Hisada, Int. J. Numer. Method Biomed. Eng. **32**, e02753 (2016).
[5] J. J. Rice, F. Wang, D. M. Bers, and P. P. de Tombe, Biophys. J. **95**, 2368 (2008).
[6] A. Landesberg and S. Sideman, Am. J. Physiol. **267**, H779 (1994).
[7] M. V. Razumova, A. E. Bukatina, and K. B. Campbell, J. Appl. Physiol. **87**, 1861 (1999).
[8] P. J. Hunter, A. D. McCulloch, and H. E. D. J. ter Keurs, Prog. Biophys. Mol. Biol. **69**, 289 (1998).
[9] J. A. Negroni and E. C. Lascano, J. Mol. Cell. Cardiol. **45**, 300 (2008).
[10] F. Jülicher and J. Prost, Phys. Rev. Lett. **78**, 4510 (1997).
[11] S. Günter and K. Kruse, New J. Phys. **9**, 417 (2007).
[12] D. Oriola, H. Gadêlha, C. Blanch-Mercader, and J. Casademunt, Europhys. Lett. **107**, 18002 (2014).
[13] S. Günter and K. Kruse, Chaos **20**, 045122 (2010).
[14] M. Kaya and H. Higuchi, Science **329**, 686 (2010).
[15] T. Q. P. Uyeda, P. D. Abramson, and J. A. Spudich, Proc. Natl. Acad. Sci. USA **93**, 4459 (1996).
[16] M. A. Geeves and K. C. Holmes, Adv. Protein Chem. **71**, 161 (2005).
[17] J. R. Sellers and C. Veigel, Nat. Struct. Mol. Biol. **17**, 590 (2010).
[18] K. W. Saupe, F. R. Eberli, J. S. Ingwall, and C. S. Apstein, Am. J. Physiol. **276**, H1715 (1999).
[19] C. W. Gardiner, *Handbook of Stochastic Methods for Physics, Chemistry and the Natural Sciences*, 3rd ed., Springer Series in Synergetics Vol. 13 (Springer-Verlag, Berlin, 2004).
[20] R. S. Varga, *Matrix Iterative Analysis* (Prentice-Hall, Englewood Cliffs, New Jersey, 1962).
[21] L. Debernard, G. E. Leclerc, L. Robert, F. Charleux, and S. E. Bensamoun, J. Musculoskelet. Res. **16**, 1350008 (2013).
[22] M. Capitanio, M. Canepari, M. Maffei, D. Beneventi, C. Monico, F. Vanzi, R. Bottinelli, and F. S. Pavone, Nat. Methods **9**, 1013 (2012).
[23] T. Erdmann and U. S. Schwarz, Phys. Rev. Lett. **108**, 188101 (2012).
[24] M. E. De Winkel, T. Blange, and B. W. Treijtel, J. Muscle Res. Cell Motil. **15**, 130 (1994).
[25] http://www.netlib.org/lapack/
[26] H. L. Sweeney and A. Houdusse, Annu. Rev. Biophys. **39**, 539 (2010).